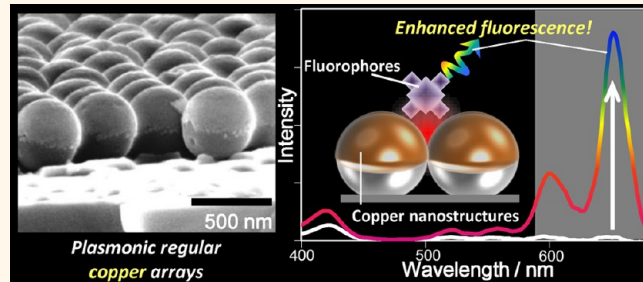


Metal-Enhanced Fluorescence Platforms Based on Plasmonic Ordered Copper Arrays: Wavelength Dependence of Quenching and Enhancement Effects

Kosuke Sugawa,^{†,*} Takahiro Tamura,[†] Hironobu Tahara,[‡] Daisuke Yamaguchi,[†] Tsuyoshi Akiyama,[§] Joe Otsuki,[†] Yasuyuki Kusaka,[†] Nobuko Fukuda,[†] and Hirobumi Ushijima[†]

[†]Department of Materials and Applied Chemistry, College of Science Technology, Nihon University, Chiyoda, Tokyo 101-8308, Japan, [‡]Division of Chemistry and Materials Science, Graduate School of Engineering, Nagasaki University, Nagasaki 852-8131, Japan, [§]Department of Materials Science, School of Engineering, The University of Shiga Prefecture, Hikone, Shiga 522-8583, Japan, and [†]Flexible Electronics Research Center, National Institute of Advanced Industrial Science and Technology (AIST), Tsukuba, Ibaraki 305-8565, Japan

ABSTRACT Ordered arrays of copper nanostructures were fabricated and modified with porphyrin molecules in order to evaluate fluorescence enhancement due to the localized surface plasmon resonance. The nanostructures were prepared by thermally depositing copper on the upper hemispheres of two-dimensional silica colloidal crystals. The wavelength at which the surface plasmon resonance of the nanostructures was generated was tuned to a longer wavelength than the interband transition region of copper (>590 nm) by controlling the diameter of the underlying silica particles. Immobilization of porphyrin monolayers onto the nanostructures was achieved *via* self-assembly of 16-mercaptophexadecanoic acid, which also suppressed the oxidation of the copper surface. The maximum fluorescence enhancement of porphyrin by a factor of 89.2 was achieved as compared with that on a planar Cu plate (CuP) due to the generation of the surface plasmon resonance. Furthermore, it was found that while the fluorescence from the porphyrin was quenched within the interband transition region, it was efficiently enhanced at longer wavelengths. It was demonstrated that the enhancement induced by the proximity of the fluorophore to the nanostructures was enough to overcome the highly efficient quenching effects of the metal. From these results, it is speculated that the surface plasmon resonance of copper has tremendous potential for practical use as high functional plasmonic sensor and devices.



KEYWORDS: localized surface plasmon resonance · copper nanostructures · fluorescence · metal-enhanced fluorescence · quenching · porphyrin · interband transition

Fluorescence-based detection is one of the most popular sensing techniques employed in the areas of biotechnology and life sciences. Therefore, enhancement of the fluorescence intensity that can be achieved from fluorophores is highly important for improving their sensitivity and achieving lower detection limits. Metal-enhanced fluorescence (MEF) is an optical phenomenon induced by the localized surface plasmon resonance (LSPR) of metal nanostructures. Because of its great potential, it has received considerable attention in many different research areas.^{1–4} Excitation enhancements and increases in the radiative decay rate of fluorophores can be achieved by

the generation of highly confined local electric fields that are induced by the LSPR, leading to dramatically improved fluorescence intensities.^{1–5} In addition, the LSPR effects cause a decrease in the excited-state lifetime and thus an increase in the photostability of the fluorophores.^{6–8} Therefore, the MEF phenomenon has a great potential to be exploited for highly sensitive bioanalytical applications such as DNA sensing,^{9–15} RNA sensing,¹⁶ immunoassays,^{17,18} and fluorescence-based imaging.^{19–21} On the other hand, the fluorescence of fluorophores located close to metal surfaces could be quenched by energy and/or electron transfer from their excited state.^{22–24} It has been reported that the

* Address correspondence to sugawa.kosuke@nihon-u.ac.jp.

Received for review July 29, 2013 and accepted October 3, 2013.

Published online October 03, 2013
10.1021/nn403925d

© 2013 American Chemical Society

magnitude of the fluorescence enhancement and quenching is mainly dependent on the distance between the fluorophores and the surface of metal nanostructures at nanometer level. They have different nonlinear distance dependences. Typically, if the distance between them is <5 nm, the fluorescence is efficiently quenched.^{25–28} In contrast, at larger distances (7–20 nm), efficient enhancement could be achieved.^{25–31} These unique spatial optical properties provide further possibilities for use in the development of novel highly sensitive biological sensors.^{9,12}

To date, the metallic species used for the fabrication of MEF-responsive plasmonic nanostructures have been limited to Au and Ag. The relatively high cost of these materials imposes a major obstacle for the practical use of plasmonic sensing devices. In contrast, Cu is significantly cheaper than both of these metals, in addition to being easy to recycle. Therefore, the realization of MEF based on the LSPR of Cu nanostructures has a tremendous potential for practical use.

Despite the great promise of Cu nanoparticles or nanostructures for MEF-based applications, there have been few reports regarding its use.³² While normal spherical Cu nanoparticles generate LSPR at around 580 nm,^{33–36} electronic interband transitions from the valence band to the Fermi level in Cu occur at a wavelength below approximately 590 nm.^{37–41} Therefore, overlap between the LSPR and the interband transition leads to damping of LSPR of the Cu nanoparticles,^{40,41} and as a result, fluorescence from the close-proximity fluorophores would be significantly quenched. Geddes *et al.* reported that fluorescence from acridine orange, which emits at approximately 520 nm, was effectively enhanced when located close to Cu nanostructures fabricated by thermal deposition.³² In another report, it was shown that the emission from CdSe/ZnS quantum dots, which emit around 585 nm, was drastically quenched when they were located near Cu nanospheres.⁴² In addition, the occurrence of quenching of fluorescence from cyanine dyes located close to Cu nanoparticles has been reported.⁴³ In these previous studies, the excitation and fluorescence wavelengths of fluorophores used were within the interband transition region of Cu, so it is highly possible that local electric fields based on Cu nanostructures were not effectively utilized because of LSPR damping. One approach to avoiding such LSPR damping is to shift the generating wavelength of Cu LSPR from the interband transition region.

There have been some recent reports on successful shifting of the LSPR to a longer wavelength region (>590 nm) by controlling the shape of the Cu nanoparticles dispersed in solution phase.^{38,39,44} However, it is difficult to remove the Cu oxide layers, which would greatly influence the optical responses of copper nanoparticles in the system consisting of the Cu nanoparticles dispersed in solutions.³⁸ On the other hand, when a nanostructured solid surface is used, the Cu

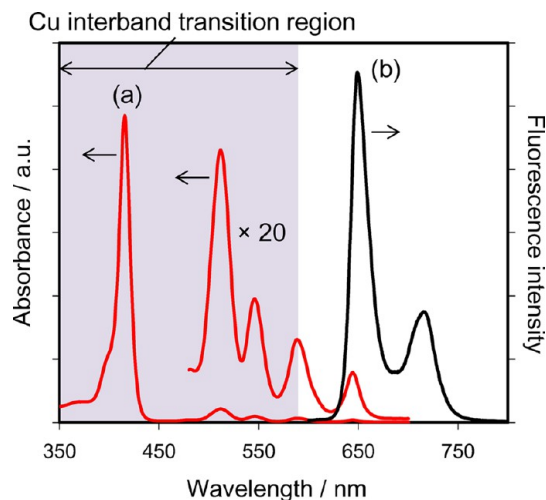


Figure 1. (a) Absorption and (b) fluorescence ($\lambda_{\text{ex}} = 415$ nm) spectra of porphyrin molecules (5,10,15,20-tetra(4-carboxyphenyl)porphyrin) in an ethanol solution. The purple-shaded area indicates the wavelength region where the interband transition of Cu metal occurs.

oxide layers can be easily removed by immersion in glacial acetic acid for *ca.* 20 s.^{45–47} It has also been shown that the immobilization of self-assembled monolayers (SAMs) consisting of long chain alkanethiol molecules onto the Cu surface can effectively suppress oxide formation.^{48–50} There have been a limited number of reported examples of Cu nanostructured substrates with a LSPR wavelength longer than the interband transition.^{41,47} For example, Van Duyne *et al.* reported that Cu nanoprisms fabricated by nanosphere lithography showed a LSPR peak around 710 nm.⁴⁷ Because of the potential of MEF-responsive plasmonic surfaces for various biological sensing applications, further investigation into their fabrication and resulting properties would be extremely useful.

In this study, we report the effective enhancement and quenching of the fluorescence from dye molecules located close to plasmonic unoxidized pure Cu nanostructures with a precisely controlled LSPR at a longer wavelength than that of the interband transition. Utilization of unoxidized Cu nanostructures is expected to facilitate the evaluation of the LSPR phenomenon and the substrate properties. This study provides a new insight into the MEF properties of plasmonic nanostructures composed of this low-cost metallic species, and so is highly useful for the practical application of plasmonic sensing devices.

RESULTS AND DISCUSSION

The porphyrin molecule used as a fluorescent probe in this study is known to exhibit prominent excitation peaks at around 420 nm (Soret band) and 520, 550, 600, and 650 nm (Q-band), and fluorescence peaks at around 650 and 710 nm (Figure 1). Therefore, these characteristic optical properties allow us to investigate the fluorescence properties throughout the Cu interband transition and surrounding regions in detail. It has been found that the use of the ordered metal half-shell arrays

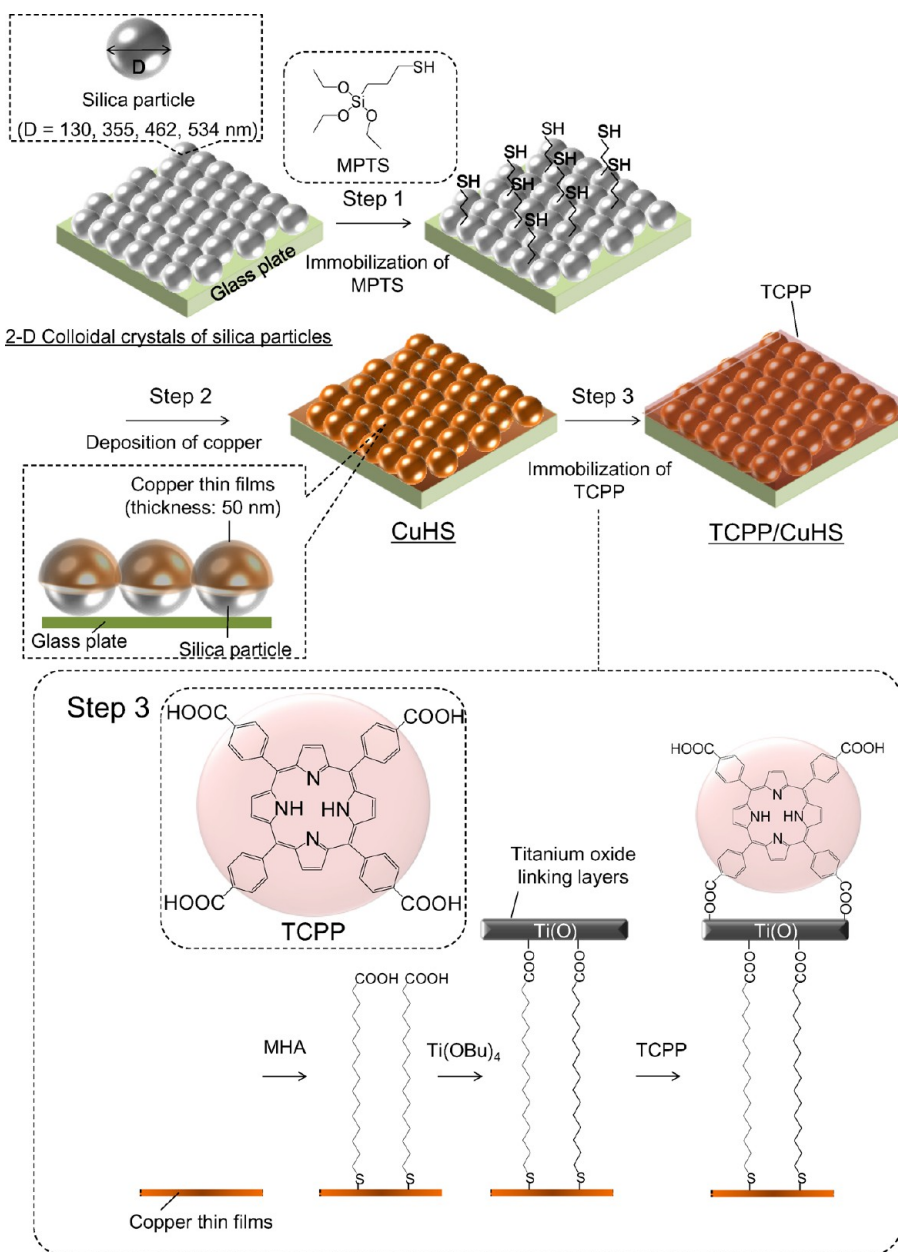


Figure 2. Schematic showing the fabrication of the CuHS arrays with immobilized TCPP fluorescence probe.

pioneered by Van Duyne's group,⁵¹ where Au and Ag are deposited on the surface of two-dimensional (2D) colloidal crystals, enables precise tuning of the LSPR wavelength from the visible to near-infrared region by changing the diameter of the underlying colloidal crystal particles.^{52–54} Therefore, it is expected that the LSPR wavelength of Cu half-shell (CuHS) arrays could be shifted away from the interband transition region.

Characterization of CuHS Arrays. Figure 2 shows a schematic of the fabrication of the CuHS arrays and the subsequent immobilization of the fluorescence probe, 5,10,15,20-tetrakis(4-carboxyphenyl)porphyrin (TCPP), onto the Cu surfaces. Full details of the experimental protocol can be found in the Materials and Methods section. The colloidal butanol solutions of silica with

four different diameters were synthesized using the Stöber method (average diameters: 130 ± 4 , 355 ± 10 , 462 ± 10 , and 534 ± 11 nm).⁵⁵ These were added to a dish of pure H₂O, where they self-assembled on the surface of the liquid. The particles were then transferred to the surface of a clean glass plate by placing it in contact with the H₂O, resulting in the formation of 2D colloidal crystals of silica.⁵⁶ After annealing them at 500 °C for 1 h, morphological evaluation of the particle layers was performed using scanning electron microscopy (SEM). As shown in Figure S1 (Supporting Information), it was confirmed that all of the different sizes of silica particles formed well-organized 2D close-packed hexagonal arrays, and that the periodic structures were present over the entire glass surface.

As shown in Figure S2 (Supporting Information), the extinction spectra of the silica colloidal crystals with diameters of 355, 462, and 534 nm showed clear diffraction peaks (stop bands) at around 415, 540, and 630 nm, respectively. These can be explained by Bragg's diffraction law ($\lambda_{\text{max}} = 2d \sin \theta / d$; d : pore distance, λ_{max} : wavelength of extinction peak),⁵⁷ suggesting the formation of a high-quality subwavelength structural periodicity. In contrast, no clear peaks were observed for the colloidal crystals of 130 nm silica particles (Figure S2, Supporting Information). This is because the stop band of these crystals is expected to appear at approximately 150 nm according to Bragg's law, and therefore the band may be generated below the spectral region probed. In addition, it was confirmed that the peak intensity and wavelength position of the extinction peak were the same for any position on the glass surface, for the samples with 355, 462, and 534 nm diameter particles; this indicates the presence of a uniform array over the entire surface.

In order to fabricate the CuHS arrays, Cu (thickness: 50 nm) were thermally deposited onto the surface of the 2D silica colloidal crystals with the four different diameters 130, 355, 462, and 534 nm, denoted as CuHS(130), CuHS(355), CuHS(462), and CuHS(534), respectively (Figure 2, step 2). In order to increase the adhesion between the Cu thin film and the silica surface, a monolayer of 3-mercaptopropyltriethoxysilane (MPTS) was immobilized on the silica surface *via* a silane coupling reaction prior to the deposition process (Figure 2, step 1).⁵⁸ The resulting CuHS arrays were found to have excellent morphological stability to the solutions used for subsequent immobilization of the fluorescent probe. SEM images of the prepared CuHS samples are shown in Figure 3. For all of the CuHS arrays, the formation of relatively smooth Cu films on the surfaces of the upper hemispheres of the silica particles can be observed over the entire substrate. These results demonstrate that high-quality CuHS arrays with morphological stability were formed over an area as large as 5 cm².

In order to evaluate the quantity of light that is absorbed by CuHS(462) after transferring from the deposition chamber to the atmosphere ($A = 1 - T - R$), both transmittance $T(\lambda)$ and reflection $R(\lambda)$ were measured (Figure 4).^{52,53} The resultant spectroscopic properties were similar to those of silver half-shell arrays in a previous report.⁵⁹ Typically, a prominent transmission peak ascribed to extraordinary optical transmission was observed at around 590 nm. And a strong absorption peak was exhibited at around 680 nm, which is consistent with the minimum of the reflectance spectrum. Furthermore, this peak is not observed in the spectra of the smooth Cu films. Thus, the observed absorption band can be attributed to the excitation of strongly localized surface plasmon.⁵⁹

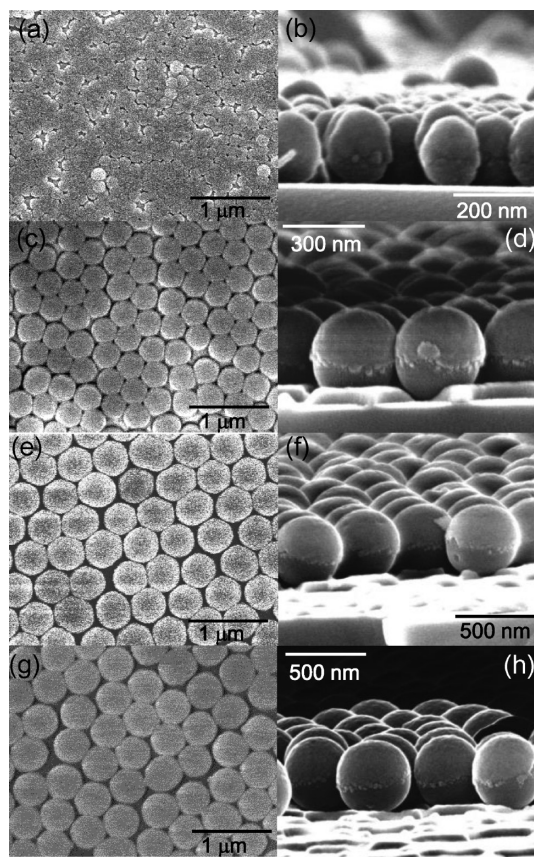


Figure 3. SEM images: top view of (a) CuHS(130), (c) CuHS(355), (e) CuHS(462), and (g) CuHS(534); and cross-sectional view of (b) CuHS(130), (d) CuHS(355), (f) CuHS(462), and (h) CuHS(534).

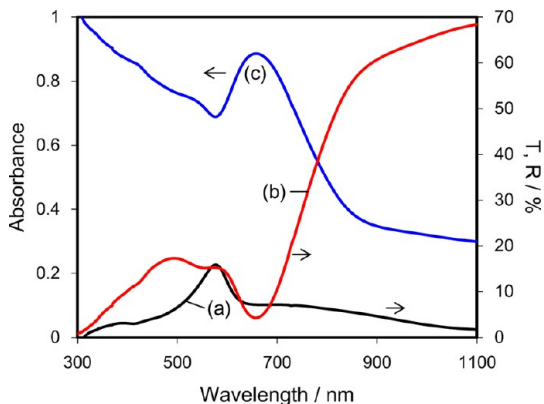


Figure 4. (a) Transmittance, (b) reflectance, and (c) inferred absorption spectra of CuHS(462).

Surface Analysis of TCPP-Modified CuHS Arrays. The surface of metallic copper is prone to oxidation upon exposure to ambient conditions, resulting in the formation of a layer consisting mainly of Cu₂O, with CuO as a minor component.^{47,60,61} In order to evaluate the surface composition of the arrays, X-ray photoelectron spectroscopy (XPS) was carried out using a monochromatized Mg K α (1253.6 eV) X-ray source. As shown in Figure 5(A), the XPS survey spectrum for the surface of

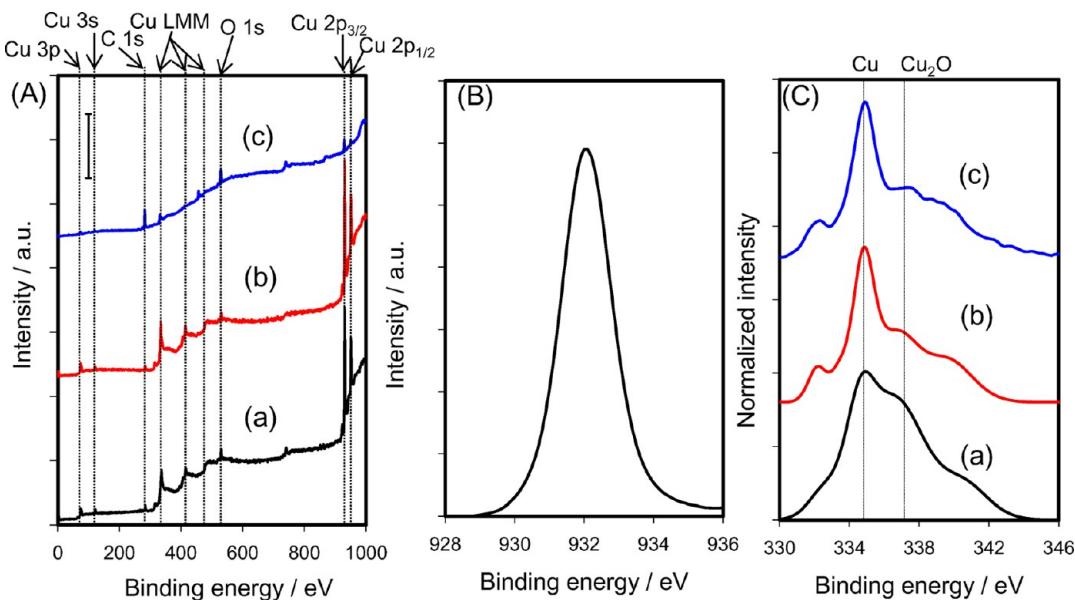


Figure 5. XPS spectra: (A) survey spectra of the surface of CuHS(462) (a) before and (b) after immersing in glacial acetic acid, and (c) after immobilization of TCPP by surface sol–gel process. (B) Cu 2p_{3/2} narrow spectrum of CuHS(462). (C) Cu LMM Auger spectra of CuHS(462) (a) before and (b) after immersing in glacial acetic acid, and (c) after immobilization of TCPP.

CuHS(462) (a) exhibits a Cu 2p doublet (Cu 2p_{1/2} and Cu 2p_{3/2}) at 952 and 932 eV, a Cu 3s peak at 123 eV, and a Cu 3p peak at 77 eV. In addition, an Auger Cu LMM triplet was observed at 335, 415, and 486 eV. The O 1s peak that is observed at 531 eV may be attributed to oxidation of Cu and adventitious contamination from the atmosphere. The presence of C 1s peak at 284 eV can also be attributed to contamination. For quantitative evaluation of the oxidation state of the surface of the arrays, high-resolution spectra were acquired for the 928–936 eV (Figure 5(B)) and 330–346 eV regions (Figure 5(C)). In the 928–936 eV region, a single peak derived from Cu 2p_{3/2} is seen at 932.2 eV. If CuO were present on the sample surface, an additional peak due to the Cu 2p_{3/2} of CuO should be present at around 934 eV.^{62,63} The absence of such a peak suggests that there was no CuO on the surface of the array. However, it is not clear whether the peak at around 932 eV is due to metallic Cu or Cu₂O, as the binding energies of the Cu 2p_{3/2} peaks derived from these two species are very similar.^{62,63} Hence, the peak can be assigned to metallic Cu, Cu₂O, or a combination of the two. After confirming the absence of CuO, the presence of Cu₂O was verified from the LMM Auger spectrum.⁶³ From spectrum (a) in Figure 5(C), it can be concluded that both metallic Cu (335.1 eV) and Cu₂O (337.2 eV) were present on the surfaces. It has been reported that the presence of Cu₂O on Cu surfaces strongly affects the LSPR properties (intensity and wavelength location) of Cu nanostructures.^{46,47} In order to investigate the precise LSPR properties of the pure CuHS arrays, the Cu₂O was removed by immersing the substrates in glacial acetic acid. Previous reports have demonstrated that this can effectively remove Cu oxides by the

following reactions, without affecting the metallic Cu: $\text{CuO} + 2\text{CH}_3\text{COOH} \rightarrow \text{Cu}(\text{CH}_3\text{COO})_2 + \text{H}_2\text{O}$ and $\text{Cu}_2\text{O} + 4\text{CH}_3\text{COOH} \rightarrow 2\text{Cu}(\text{CH}_3\text{COO})_2 + \text{H}_2\text{O} + \text{H}_2$.⁴⁷ In the narrow spectrum ((b) in Figure 5(C)) for the CuHS(462) after immersion in glacial acetic acid for 40 s, the peak from Cu₂O has almost disappeared, with a concurrent increase in the peak for metallic Cu. In addition, it was confirmed that the cupric acetate formed by the treatment with glacial acetic acid did not remain on the Cu surfaces because the Cu 2p_{3/2} peak from cupric acetate was not observed from XPS measurement after the treatment. These results suggest that CuHS arrays consisting of high purity metallic Cu were successfully fabricated *via* simple treatment with glacial acetic acid. From the absorption spectra (Figure 6), a blue shift in the LSPR peak wavelength of the arrays was observed from 690 to 675 nm after immersing in acetic acid. This peak shift was likely caused by the removal of the Cu₂O thin layers, as previously reported.^{46,47} Meanwhile, we confirmed that removal of the Cu₂O did not substantially affect the structural geometry of the CuHS arrays by the SEM observation.

In this study, TCPP fluorescent probe molecules were immobilized on the surface of the CuHS arrays by a combination of self-assembly and a surface sol–gel process (Figure 2, step 3).⁶⁴ First, SAMs of 16-mercaptohexadecanoic acid (MHA) were formed on the surfaces of the CuHS arrays. Previous reports have demonstrated that the progress of Cu oxidation can be dramatically suppressed by coating with protective layers consisting of long alkanethiols.^{48–50} For the CuHS arrays fabricated in the present study, it was confirmed from the LMM Auger spectra that the Cu surface without the MHA SAM oxidized rapidly over the

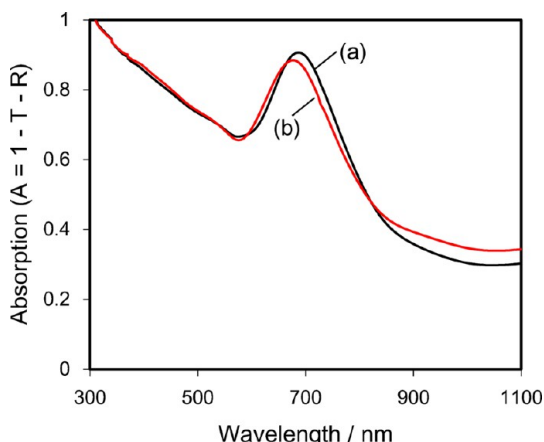


Figure 6. Absorption spectra ($A(\lambda) = 1 - T(\lambda) - R(\lambda)$) of CuHS(462) (a) before and (b) after immersing in glacial acetic acid.

course of 1 h, whereas the SAM-modified surface was protected from oxidation for at least 3 h (Figure S3, Supporting Information). Immobilization of TCPP was subsequently achieved using a surface sol–gel process *via* the formation of titanium oxide linking layers to form the TCPP-modified CuHS samples (TCPP/CuHS).^{64–67} The LMM Auger spectrum from the obtained TCPP/CuHS shows that very little oxidation of the Cu surface occurred during the TCPP immobilization process ((c) in Figure 5(C)). These results demonstrate the successful fabrication of hybrids composed of a fluorescent probe molecule and highly pure Cu nanostructures, without any oxide layer.

LSPR Properties and Fluorescence Enhancement of TCPP/CuHS Arrays. The LSPR properties of each of the fabricated TCPP/CuHS arrays were next investigated. A CuP modified with TCPP molecules was also prepared in the same manner as for the TCPP/CuHS arrays as a control substrate (TCPP/CuP). Absorption spectra for the TCPP/CuHS and TCPP/CuP are shown in Figure 7. The spectrum for TCPP/CuP shows a very broad band below around 590 nm derived from electronic interband transitions from the valence band to the Fermi level of metallic Cu.^{38,39} For TCPP/CuHS(130), only a weak absorption peak at 575 nm can be observed. It is known that the LSPR from Cu nanospheres occurred at around 580 nm^{33–36} and overlaps with the interband transition bands.^{32,37–41} As a result, the interband transitions can efficiently damp the LSPR through dephasing of the optical polarization associated with the electron oscillation.^{38–41} Therefore, the results acquired here suggest that the LSPR generated on TCPP/CuHS(130) was damped by the effect of the interband transitions. In contrast, the spectrum from TCPP/CuHS(355) shows a prominent LSPR absorption peak at 630 nm; the peaks become red-shifted to longer wavelength regions as the diameter of the underlying silica particles increased (TCPP/CuHS(462): 675 nm, TCPP/CuHS(534): 715 nm). Therefore, these results suggest that the LSPR properties of the

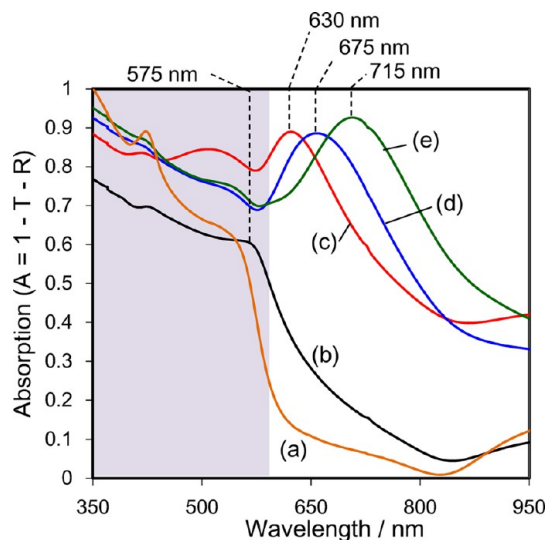


Figure 7. Absorption spectra ($A(\lambda) = 1 - T(\lambda) - R(\lambda)$) of (a) TCPP/CuP, (b) TCPP/CuHS(130), (c) TCPP/CuHS(355), (d) TCPP/CuHS(462), and (e) TCPP/CuHS(534). The purple-shaded area indicates the wavelength region where the interband transition of Cu metal occurs.

TCPP/CuHS are qualitatively similar to those of Au and Ag half-shell arrays.^{52,53} The present results demonstrate that the wavelength at which LSPR is generated was successfully shifted to a longer wavelength region than that of the Cu interband transition (<590 nm); precise tuning of the LSPR wavelength is possible by varying the size of the underlying silica particles.

The number of TCPP molecules immobilized on each substrate was experimentally estimated, as described in the Materials and Methods. The coverages of TCPP on CuHS(130, 355, 462, and 534) and CuP were calculated to be 2.39×10^{-10} , 2.41×10^{-10} , 2.39×10^{-10} , 2.24×10^{-10} , and 1.87×10^{-10} mol/cm² (flat exposed area), respectively. Assuming that Cu was deposited on the upper hemispheres of the 2D silica colloidal crystals, as observed in the SEM images (Figure 3), the total exposed area of the Cu thin films of the CuHS was calculated to be *ca.* 1.6 times larger than the exposed flat surface area (CuP). Therefore, the number of TCPP molecules immobilized on the CuHS should also be *ca.* 1.6 times larger than that on the CuP. The ratio of the number of TCPP on the CuHS to that on the CuP was found experimentally to be 1.2–1.3, which is somewhat lower than the calculated estimation. This may be due to a decrease in the area exposed because of points of contact between adjoining silica particles. Assuming that the area of a TCPP molecule with parallel packing on the Cu surface is 1.5 nm², the theoretical full coverage was calculated to be 8.6×10^{-11} mol/cm² (flat exposed area).⁶⁸ On the other hand, if one assumes 0.4 nm thickness for the plane of TCPP with perpendicular packing, the full coverage is calculated to be 3.0×10^{-10} mol/cm² (flat exposed area).⁶⁸ These results imply that TCPP molecules were immobilized *via* the surface

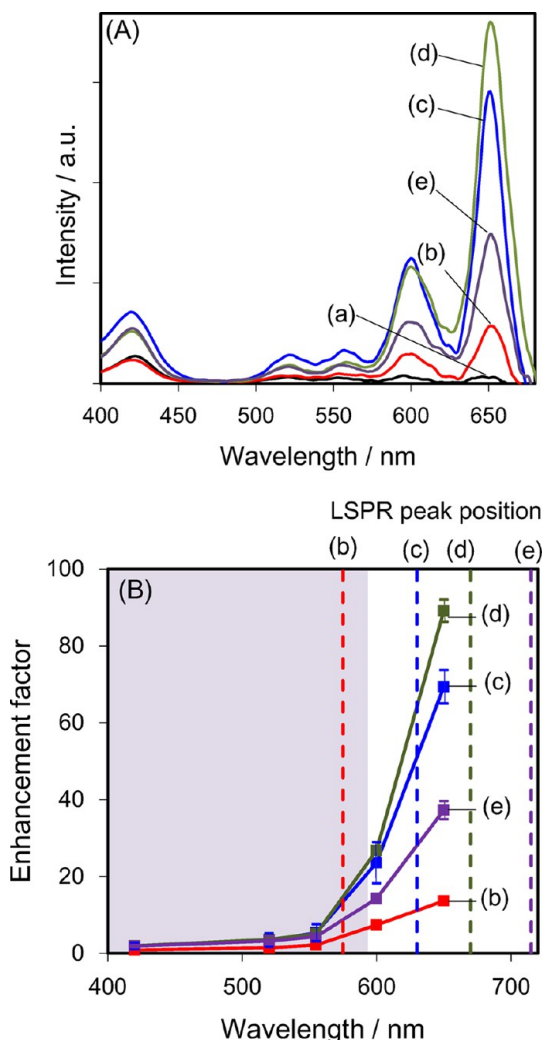


Figure 8. (A) Fluorescence excitation spectra ($\lambda_{\text{em}} = 715$ nm) of (a) TCPP/CuP, (b) TCPP/CuHS(130), (c) TCPP/CuHS(355), (d) TCPP/CuHS(462), and (e) TCPP/CuHS(534). (B) plots of EF of fluorescence intensity from (b) TCPP/CuHS(130), (c) TCPP/CuHS(355), (d) TCPP/CuHS(462), and (e) TCPP/CuHS(534) against that of TCPP/CuP at 420, 520, 555, 600, and 650 nm, together with the LSPR peak position of each sample (dashed line), (b) TCPP/CuHS(130), (c) TCPP/CuHS(355), (d) TCPP/CuHS(462), and (e) TCPP/CuHS(534). The purple-shaded area indicates the wavelength region where the interband transition of Cu metal occurs. Average values obtained from three different samples are plotted, and the standard deviation is indicated with an error bar.

sol-gel method formed an almost monolayer structure on the Cu surface, with the porphyrin ring adopting a tilted or random-tilted configuration at various angles to the Cu surface.

Fluorescence excitation spectra of the TCPP/CuHS and TCPP/CuP samples were measured at $\lambda_{\text{em}} = 715$ nm. The spectra were corrected for the differences in the estimated number of immobilized TCPP molecules on the surfaces. In order to remove the light scattering effect of the Cu substrates, the spectra of the CuHS and CuP before modification with TCPP were subtracted. The obtained spectra are shown in Figure 8(A). The fluorescence peaks derived from the radiative

TABLE 1. Detailed Values of EF Calculated from Figure 8(B)

fluorescence peak wavelength (nm)	enhancement factor			
	TCPP/ CuHS(130)	TCPP/ CuHS(355)	TCPP/ CuHS(462)	TCPP/ CuHS(534)
420	0.8	1.9	1.9	1.9
420	1.4	3.4	3.6	3.2
555	2.2	5.3	5.1	4.3
600	7.4	23.6	26.8	14.3
650	13.7	69.3	89.2	37.2

process of excited TCPP were observed at around 420, 520, 555, 600, and 650 nm. It appears that longer excitation wavelengths afforded more pronounced fluorescence. In order to verify these results, the enhancement factor (EF) of the fluorescence intensity of the five peaks for each TCPP/CuHS was plotted against that for TCPP/CuP (Figure 8(B)), and the numerical EF values are shown in Table 1. It can be seen in Figure 8(B) that while the fluorescence intensity of the three peaks (420, 520, and 555 nm) in the shorter wavelength region that overlaps with the interband transition bands of Cu did not vary significantly with the diameter of the underlying silica nanospheres, the intensities of the peaks at 600 and 650 nm, which are above the interband transition bands, changed drastically. For the peak at 420 nm, while the fluorescence intensity of TCPP/CuHS(130) was found to be almost the same as for TCPP/CuP, those of TCPP/CuHS(355, 462, and 534) were slightly enhanced (Table 1). It has been reported that the fluorescence enhancement from fluorophores located near to metal nanostructures is attributable to two contributions:^{1–5} (1) excitation enhancement due to strong local electric fields associated with the excitation of LSPR, and (2) increase in the radiative decay rate from a surface plasmon resonance-coupled excited state of the fluorophore.^{1–5} Therefore, the fluorescence enhancement is very sensitive to the degree of spectral overlap between the LSPR bands and the excitation and the emission wavelengths of the fluorophore.^{53,69} The observed emission wavelength ($\lambda_{\text{em}} = 715$ nm) in this measurement overlaps with the LSPR bands from TCPP/CuHS(355, 462, and 534). Thus, fluorescence enhancement could occur because of an increase in the radiative decay rate of excited TCPP, but the actual EF values were only moderate when excited at 420, 520, and 555 nm, as all three excitation wavelengths are located in the wavelength region of the interband transition of Cu. On the other hand, for all samples but TCPP/CuHS(130), the EF values at 600 nm, which is a moderately longer wavelength than the interband transition band, were extremely larger than those at 420, 520, and 555 nm. Furthermore, the EF values at the even longer wavelength of 650 nm became even larger, with a maximum value of 89.2 achieved for the TCPP/CuHS(462).

The order of the EF values at this wavelength was TCPP/CuHS(462) > TCPP/CuHS(355) > TCPP/CuHS(534) > TCPP/CuHS(130). There are two possible reasons why the EF value for TCPP/CuHS(130) was lowest for both excitation wavelengths of 600 and 650 nm. First, the LSPR band (peak position: red dashed line (b) in Figure 8(B)) only barely overlaps with both the excitation wavelength (650 nm) and fluorescence wavelength (715 nm), and therefore, there was less induction of an enhancement in excitation and emission from the TCPP immobilized on the CuHS(130). Second, excitation of the LSPR from the TCPP/CuHS(130) was efficiently damped by the significant overlapping between the LSPR band and the interband transition of Cu (Figure 7(b)).⁴⁰ For the TCPP/CuHS(462), on the other hand, LSPR damping was inhibited by tuning the LSPR peak wavelength to achieve a value above the interband transition. In addition, the LSPR band overlapped with both the excitation and the fluorescence wavelengths (green dashed line (d) in Figure 8(B)). Thus, the excitation and the emission processes from TCPP immobilized on CuHS(462) were effectively enhanced, resulting in the generation of considerably higher fluorescence intensity. While the TCPP/CuHS(355 and 534) also showed LSPR peaks above the interband transition (blue (c) and purple (e) dashed lines in Figure 8(B), respectively), the LSPR bands did not efficiently overlap with the excitation and/or emission wavelengths. As such, reduction in the spectral overlap could moderately decrease the EF, compared to that of the TCPP/CuHS(462).

It has been reported that the gold half-shell arrays generate strong electric fields (hot sites) at the gap between the two adjacent particles.⁷⁰ In order to probe the relevance to our system, finite difference time domain (FDTD) calculations were carried out for CuHS-*d* (*d* = 355, 462, 534 nm) to estimate electric field distributions at the hot sites. The detailed calculation models are shown in the Supporting Information. Figure 9 shows the typical electric field distribution on the surface of CuHS(462) under the irradiation of 650 nm incident light. The electric field enhancement factors at hot sites of CuHS(*d*) were 840 (*d* = 355 nm), 1100 (*d* = 462 nm) and 680 (*d* = 534 nm) at 650 nm, respectively. Therefore, the order of enhancement factor with respect to the diameter of the silica particles agreed with experimentally observed order of fluorescence enhancement. From these results, we have demonstrated that prominent generation of Cu LSPR that is not affected by the interband transition can efficiently enhance the fluorescence of fluorophores located close to Cu nanostructures. The calculated field enhancement factors are quite different from the experimental results because only the fluorescence from TCPP immobilized within the hot site regions was effectively enhanced.

Fluorescence Quenching and Enhancement of TCPP on CuHS Arrays. Metal surfaces are also known to be strong quenchers of molecular excited states.^{22–24,28,42,43}

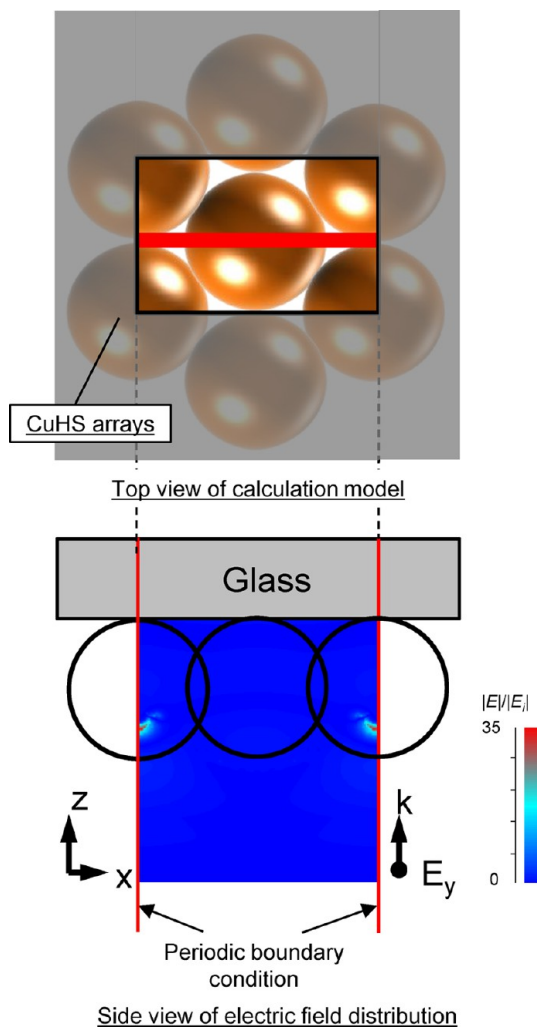


Figure 9. Electric field distribution of CuHS(462) irradiated by *y*-polarized incident light of 650-nm wavelength.

Thus, the practical usefulness of fluorescence enhancement of fluorophores based on the LSPR effects is dependent on the results of competition between the enhancement and the quenching effects. In order to verify the competition between enhancement and quenching for the Cu LSPR, the fluorescence excitation spectra of TCPP/CuHS(462), TCPP/CuP, and TCPP immobilized on a glass surface *via* the surface sol–gel process (denoted as TCPP/Glass) were compared. The TCPP/Glass acted as a control sample as it is free of the enhancement and quenching effect of the metal. It was prepared by attaching the Ti(OBu)_4 species to hydroxyl groups present on a glass substrate (see Materials and Methods section) and then attaching the TCPP in the same way as for the TCPP/CuHS. All of the fluorescence excitation spectra (Figure 10(A)) were corrected for the differences in the number of modified TCPP molecules. The EF values of the fluorescence signals from TCPP/CuHS(462) and TCPP/CuP were plotted against those from TCPP/Glass at the five fluorescence peaks (Figure 10(B)). The fluorescence for TCPP immobilized on CuP at all of the five wavelengths was drastically

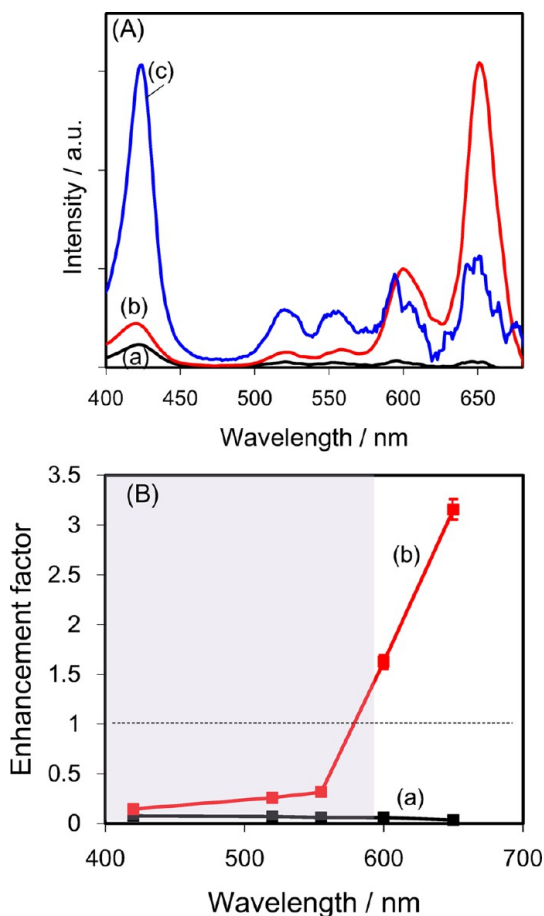


Figure 10. (A) Fluorescence excitation spectra ($\lambda_{\text{em}} = 715 \text{ nm}$) from (a) TCPP/CuP, (b) TCPP/CuHS(462), and (c) TCPP/Glass. (B) Plots of EF of fluorescence intensity of (a) TCPP/CuP and (b) TCPP/CuHS(462) against that of TCPP/Glass at 420, 520, 555, 600, and 650 nm. The purple-shaded area indicates the wavelength region where the interband transition of Cu metal occurs. Average values obtained from three different samples are plotted, and the standard deviation is indicated with an error bar.

quenched down to 1/28–1/13 in comparison to the TCPP/Glass. The quenching rate constant is determined by the dielectric losses in the metal. According to the Dulkeith *et al.*, quenching rate constant of the fluorophore is around 10^8 – 10^9 s^{-1} on gold nanoparticles.²² As the imaginary parts of the dielectric function of gold and copper around 600–750 nm are similar to each other (see Figure S4, Supporting Information),³⁷ the quenching rate constant by CuHS should be approximately on the same order as that by gold nanoparticles. The fluorescence quantum yield is described as $k_{\text{f}}/(k_{\text{f}} + k_{\text{q}})$, where k_{f} and k_{q} are the rate constants for fluorescence and quenching. The average fluorescence lifetime ($1/k_{\text{f}}$) of TCPP immobilized on the glass plate was measured to be 3.5 ns using light emitting diode (LED) light source of 405 nm excitation wavelength, which gives $k_{\text{q}} = 3.4$ – $7.7 \times 10^9 \text{ s}^{-1}$. Therefore, the fluorescence quenching ratio by CuP is reasonably accounted for by the effects of dielectric losses by Cu. For the TCPP/CuHS(462), although not to the same extent as for the

TCPP/CuP, the fluorescence signals at 420, 520, and 550 nm were also quenched down to 1/7–1/3. However, at 650 nm, which is within the LSPR band, the EF value reached 3.2. The fluorescence intensity from fluorophores immobilized on the plasmonic metal nanostructures is largely dependent on the distance between the fluorophores and metal surfaces.^{25–31} The thickness of MHA SAMs can be estimated to be between 2.0 and 2.5 nm as previously reported.^{71,72} The thickness of the linking layer is estimated to be approximately 0.36 nm (see Supporting Information), and therefore, the distance between TCPP molecules and Cu surfaces is calculated to be less than 3 nm. The estimated distance corroborates the result of efficient quenching of TCPP by CuHS (<600 nm) as well as by CuP (the whole wavelength range). Typically, energy transfer from photoexcited TCPP to Cu surfaces efficiently occur over such a small distance, leading to the fluorescence quenching of TCPP.^{28,73,74} Nonetheless, a significant enhancement of fluorescence of porphyrins was observed in our system in the wavelength range that the plasmonic effect of CuHS was present (>600 nm), which would not have been observed if the porphyrin molecules were attached directly on the Cu surface. This result suggests that the MHA SAMs and the linking layers act as an effective spacer layer.

Generality and Usability of CuHS Arrays as Metal-Enhanced Fluorescence Platforms. From these results described above, we demonstrated that the Cu LSPR generated in the wavelength region longer than the interband transition on CuHS arrays can enhance the fluorescence from TCPP molecules. Furthermore, we tried to enhance the fluorescence from another fluorophore to verify generality and usability of CuHS arrays as metal-enhanced fluorescence platforms. Indocyanine green (ICG) molecule (the chemical structure is shown in Figure 11(A)) is a commercially available near-infrared (NIR) fluorescent molecule and is used extensively as a fluorescent marker in clinical imaging.⁷⁵ However, the fluorescence quantum yield is very low (ca. 1.2%),⁷⁶ and therefore, enhancement of its fluorescence intensity is very important in clinical applications. Previous reports demonstrated that the LSPR from the noble metal nanostructures such as gold nanoshells and triangular silver nanoplates enhanced the fluorescence intensity of ICG.^{31,77,78} In this study, we demonstrate that the fluorescence from ICG is enhanced also by the Cu LSPR from CuHS arrays.

It is well-known that ICG exhibits an excitation peak around 780 nm and a fluorescence peak around 815 nm as shown in Figure 11(B) (inset). In order to produce the Cu LSPR at the NIR wavelength region, we fabricated CuHS arrays based on the 2D colloidal crystals of $585 \pm 10 \text{ nm}$ silica particles, which is larger than those used for porphyrin described above (denoted as CuHS(585), the SEM images are shown in the Supporting Information). After the MHA SAM was

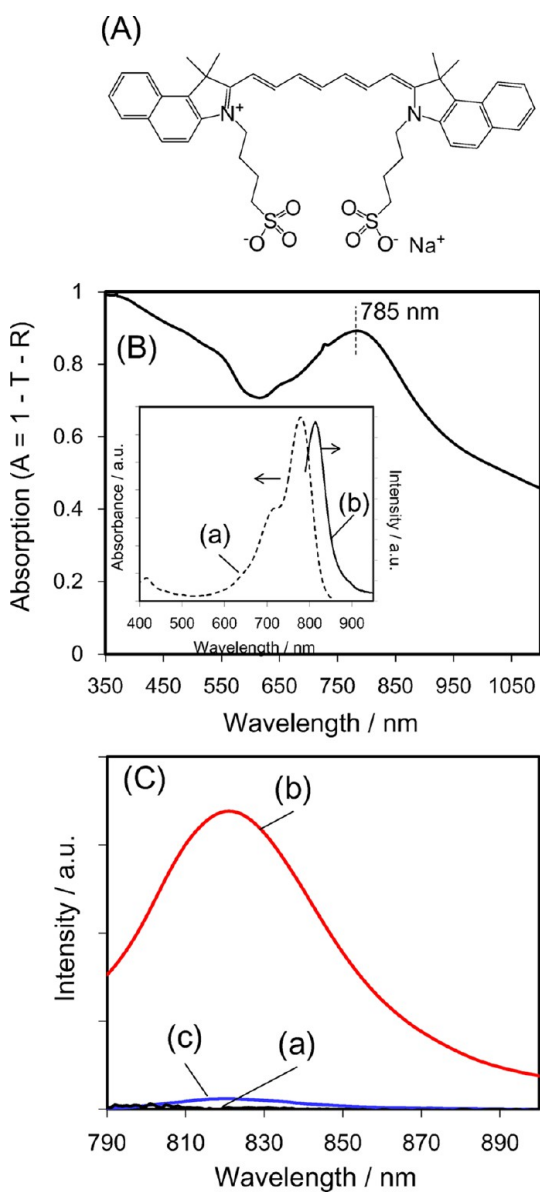


Figure 11. (A) Chemical structure of indocyanine green (ICG). (B) Absorption spectra of ICG/CuHS(585) and inset: (a) absorption spectrum and (b) fluorescence spectrum ($\lambda_{\text{ex}} = 760 \text{ nm}$) of an ICG solution. (C) Fluorescence spectra ($\lambda_{\text{ex}} = 760 \text{ nm}$) of (a) ICG/CuP, (b) ICG/CuHS(585), and (c) ICG/Glass.

formed on the CuHS(585), poly(ethylene imine) (PEI) was modified on the surface to produce the positively charged surface. The thickness of the modified PEI was estimated to be less than 1 nm as reported previously.⁷⁹ Finally, ICG molecules were immobilized on the surfaces of the CuHS(585) (denoted as ICG/CuHS(585)) utilizing electrostatic interaction between the positively charged surface and the negatively charged ICG. Similarly, ICG molecules were immobilized on the surfaces of a CuP and a glass plate as control substrates (denoted as ICG/CuP and ICG/Glass, respectively). Full details of the experimental protocol can be found in the Materials and Methods section).

As shown in Figure 11(B), the LSPR from ICG/CuHS(585) was generated at around 785 nm, which overlaps with both the excitation and fluorescence wavelengths of ICG. Therefore, it is expected that the excitation enhancement and the increase in the radiative decay rate of the excited ICG occur by the effect of Cu LSPR, leading the fluorescence enhancement of ICG. The fluorescence spectra ($\lambda_{\text{ex}} = 760 \text{ nm}$) for ICG/CuHS(585), ICG/CuP, and ICG/Glass are shown in Figure 11(C). The spectra were corrected for the differences in the estimated number of immobilized ICG molecules on the surfaces. While ICG molecules on the glass surface showed a weak fluorescence signal, those on the CuP showed no signals by the quenching effect of Cu metal. On the other hand, it is noteworthy that the fluorescence intensity from ICG on the CuHS(585) was drastically enhanced up to 28 times compared with those on the glass surface. These results strongly suggest that the plasmonic CuHS arrays are very useful as metal-enhanced fluorescence platforms.

It has been reported that Au and Ag nanostructures lead to the fluorescence enhancement of 1.4 to tens of times^{25,29–31,80–84} and 3–1000 times,^{26,27,85–90} respectively, depending on various factors including the structural morphology, the optical properties of fluorophores, the distance between nanostructure surfaces and fluorophores, and the relations between the LSPR wavelength and the excitation/emission wavelength of the fluorophore, and so on. The EFs obtained in this study lie within the ranges of variation for Au LSPR. More important, Cu is considerably cheaper than Au and Ag and easy to recycle. In addition, the surface oxidation can be easily prevented by simple surface modification such as immobilization of alkanethiol SAMs. Therefore, we have demonstrated that the Cu LSPR has tremendous potential for the practical use of MEF-based highly sensitive optical sensors.

CONCLUSIONS

We have demonstrated that the development of an ordered array of highly pure Cu nanostructures can produce significant LSPR by changing the wavelength at which it is generated to longer wavelengths away from the interband transition region. Furthermore, we have shown that the local electric fields due to the LSPR generation drastically enhanced the fluorescence signals from a porphyrin derivative above the internal transition region. The enhancement effects were able to overcome the highly efficient quenching intrinsic to metallic Cu. As controlling the distance between metal nanostructures and fluorescent molecules to tens of nanometers can efficiently suppress the quenching effect, it is expected that insertion of interlayers with an appropriate thickness could lead to further enhancement in fluorescence signals on the plasmonic Cu nanostructures. Thus, these results will

lead to the development of plasmonics that can be produced from cheaper metal species, thereby

increasing the scope of future practical applications of plasmonics.

MATERIALS AND METHODS

Materials. Milli-Q-grade water (resistivity: 18.2 MΩ·cm) was used to prepare all aqueous solutions. NH₃ aq. (28%), TEOS, 1-butanol, 2-propanol, poly(ethylene imine) (M.N. 60 000, 50 wt % aq.) and H₂O₂ (34.5%) were obtained from Kanto Chemical, Japan. Absolute ethanol (99.5 vol %), TCPP, and Ti(OBu)₄ were obtained from Wako Pure Chemical, Japan. MPTS and ICG were obtained from Tokyo Kasei, Japan, and MHA was obtained from Sigma-Aldrich. All materials were used without further purification.

Synthesis of Colloidal Solutions of Silica Particles. Silica particles with average diameters of 130 ± 4, 355 ± 10, 462 ± 10, and 534 ± 11 nm were synthesized using the Stöber method.⁵⁵ Typically, NH₃ aq. (28%) (2.2, 8.1, 11.2, or 22.6 mL, respectively) was added to absolute ethanol (26.5, 19.5, 16.7, or 14.6 mL, respectively) and stirred for 10 min at room temperature. TEOS (0.75, 1.0, 2.4, or 2.7 mL, respectively) was quickly added to the solutions, and the mixtures were stirred for 3 h. The resultant colloidal solutions of silica particles were centrifuged at 9000 rpm for 15 min and then redispersed twice in an equivalent amount of ethanol. They were then centrifuged at 9000 rpm for 15 min and redispersed twice in an equivalent amount of 1-butanol. Silica particles with diameter of 585 ± 10 nm were synthesized using a modified version of previously reported procedure.⁹¹ NH₃ aq. (4 mL) was added to absolute ethanol (20.5 mL) and stirred for 10 min. A mixed solution of absolute ethanol (0.8 mL) and TEOS (0.2 mL) was added to the solution, which was further stirred for 1 h. Then, NH₃ aq. (2 mL) and a mixed solution of absolute ethanol (11.5 mL) and TEOS (2.9 mL) was added to the solution, which was further stirred for 2 h. Finally, NH₃ aq. (2 mL) was added to the solution, which was further stirred for 2 h. The resultant colloidal silica particles were purified by centrifugation as described above and redispersed in the same amount of 1-butanol.

Fabrication of CuHS Arrays. The 2D colloidal crystals consisting of silica particles were fabricated on clean glass plates. The hydrophilic glass plates (2.0 cm × 2.5 cm) were first treated in a mixed solution of NH₃ aq./H₂O₂ aq. (1:1 v/v) at 100 °C and then washed thoroughly with H₂O. A small amount of each colloidal 1-butanol solution of the silica particles was added dropwise to ultrapure water in a Petri dish, resulting in the formation of 2D colloidal crystals of the silica particles on the water surface.⁵⁶ When the edge of a glass plate was placed in contact with this surface, the crystals were spontaneously transferred by Marangoni flow, completely covering the glass substrate. Finally, the samples were annealed at 500 °C for 1 h to physically strengthen the colloidal crystals.

The CuHS arrays were fabricated as follows. First, the silica surfaces were coated with thiol groups by immobilization of MPTS via a silane coupling reaction.⁵⁸ Typically, a mixed solution containing MPTS (1 mL), Milli-Q water (1 mL), and 2-propanol (40 mL) was refluxed for 1 h at 100 °C. After cooling the solution, the substrate containing the colloidal crystals was immersed into the solution for 30 min, followed by washing thoroughly with ethanol and drying in air at 75 °C. Finally, in order to fabricate the CuHS, 50 nm of Cu was thermally deposited under a high vacuum (7.5 × 10⁻⁷ Torr) onto the surface of the 2D colloidal crystals. As a reference sample, a planar Cu plate (CuP) was prepared by thermal deposition of Cu onto the surface of MPTS-immobilized glass plates with the same thickness as for the CuHS.

Immobilization of TCPP on CuHS Arrays. A monolayer of TCPP was immobilized on the CuHS arrays as follows.^{64–67} Briefly, ethanol solution of 1 mM MHA was degassed by bubbling N₂ through it. The as-prepared CuHS arrays were immersed in the solution for 10 h and then removed, washed with ethanol, and dried under a stream of N₂, to provide an MHA SAM on Cu surface, stabilized by strong S-metal bonding. The substrate was next immersed in a 0.1 M solution of Ti(OBu)₄ in degassed toluene for 10 min to achieve chemical bonding between the Ti compound and the

carboxyl groups on the surface of the MHA SAMs. After washing with anhydrous ethanol, the substrate was immersed in H₂O for 30 min to generate surface hydroxyl groups and then dried under a stream of N₂. Finally, the substrate was immersed in a 0.1 mM solution of TCPP in degassed ethanol for 30 min, washed with ethanol, and then dried under a stream of N₂ to produce the Cu surfaces terminating in a layer of TCPP (TCPP/CuHS). As a control sample, TCPP was immobilized on the CuP sample in the same manner (TCPP/CuP).

A TCPP/Glass control substrate was also prepared. A hydrophilic clean glass plate with hydroxyl groups on the surface was immersed in a 0.1 M solution of Ti(OBu)₄ in degassed toluene for 10 min to achieve coordinate bonding between Ti(OBu)₄ and the hydroxyl groups. The immobilization of TCPP molecules was then performed in the same manner as for the TCPP/CuHS and TCPP/CuP.

Quantitation of the Number of TCPP Molecules Immobilized on the CuHS and CuP. Substrates 2.0 cm × 2.5 cm in size were immersed in 3 mL of a 0.2 M aqueous solution of NaOH for 10 min to dissolve the surface TCPP into the solution. After this treatment, it was confirmed by measuring the absorption spectra of the sample substrates that almost all of TCPP molecules were dissolved into the solution. The absorption spectra of the aqueous solution containing TCPP were measured and the coverages of TCPP on each sample was calculated to be 2.39 × 10⁻¹⁰, 2.41 × 10⁻¹⁰, 2.39 × 10⁻¹⁰, 2.24 × 10⁻¹⁰, and 1.87 × 10⁻¹⁰ mol/cm² (flat exposed area), for the CuHS prepared with silica particles of 130, 355, 462, and 534 nm, and the CuP, respectively.

Immobilization of ICG on the CuHS Array, CuP, and Glass Plate and Quantitation of the Number of ICG Molecules. ICG molecules were immobilized on the CuHS(585) (ICG/CuHS(585)) and CuP (ICG/CuP) as follows. The MHA SAM-immobilized CuHS and CuP were immersed in a degassed aqueous solution of PEI (0.48 mg/mL) for 10 min to produce positively charged surfaces. After washing with H₂O, the substrates were immersed in a degassed ICG solution in H₂O (1 μM) for 1 h, followed by washing with H₂O, and dried under a stream of N₂. An ICG-immobilized glass control substrate (ICG/Glass) was also prepared as follows. A hydrophilic clean glass plate was immersed in the PEI solution, followed by washing with H₂O. Finally, the substrate was immersed in the ICG solution for 1 h, followed by washing with H₂O.

Quantitation of the number of ICG molecules immobilized on the substrates was performed by dissolving the surface-immobilized ICG into 2 mL of 0.15 mM aqueous solution of NaOH and measuring the absorption spectra of the solution.

Substrate Characterization. Extinction spectra were measured using a JASCO V630 UV-vis spectrophotometer. Fluorescence excitation spectra were measured using a JASCO FP-6500 spectrophotometer. Scanning electron microscopy (SEM) observations were carried out using a HITACHI S-4500 microscope. Surface analysis of Cu films on the silica colloidal crystals that were deposited by thermal evaporation, was performed using X-ray photoelectron spectroscopy (XPS) using ESCA-3400 electron spectrometer (Shimadzu Co., Japan), using a base pressure of <1.5 × 10⁻⁸ Torr and a monochromatized Mg Kα (1253.6 eV) X-ray source. Fluorescence lifetime for TCPP/Glass was measured by fluorescence lifetime spectrometer using Quantaurus-Tau (Hamamatsu Photonics). The thickness of titanium oxide linking layers was measured by tapping mode atomic force microscope (AFM) using Nanoscope IIIa (Digital Instruments).

Conflict of Interest: The authors declare no competing financial interest.

Acknowledgment. This work was supported by JSPS Grant-in-Aid for Young Scientists (B) Grant Number 24750135.

Supporting Information Available: SEM images (Figure S1) and transmission extinction spectra of 2D colloidal crystals of

silica particles (Figure S2), Cu LMM Auger spectra for CuHS(462) coated with MHA SAMs (Figure S3), dielectric function of Cu and Au (Figure S4), FDTD calculation conditions, the model of CuHS (Figure S5), AFM image of 20 layers of the titanium oxide thin films (Figure S6), SEM images of CuHS(585) (Figure S7), and discussion about the effect of radiative decay of TCPP by CuHS surface are given. This material is available free of charge via the Internet at <http://pubs.acs.org>.

REFERENCES AND NOTES

1. Lakowicz, J. R. Radiative Decay Engineering: Biophysical and Biomedical Applications. *Anal. Biochem.* **2001**, *298*, 1–24.
2. Aslan, K.; Gryczynski, I.; Malicka, J.; Matveeva, E.; Lakowicz, J. R.; Geddes, C. D. Metal-Enhanced Fluorescence: an Emerging Tool in Biotechnology. *Curr. Opin. Biotechnol.* **2005**, *16*, 55–62.
3. Lakowicz, J. R.; Ray, K.; Chowdhury, M.; Szmacinski, H.; Fu, Y.; Zhang, J.; Nowaczyk, K. Plasmon-Controlled Fluorescence: a New Paradigm in Fluorescence Spectroscopy. *Analyst* **2008**, *133*, 1308–1346.
4. Deng, W.; Goldys, E. M. Plasmonic Approach to Enhanced Fluorescence for Applications in Biotechnology and the Life Sciences. *Langmuir* **2012**, *28*, 10152–10163.
5. Xie, F.; Baker, M. S.; Goldys, E. M. Enhanced Fluorescence Detection on Homogeneous Gold Colloid Self-Assembled Monolayer Substrates. *Chem. Mater.* **2008**, *20*, 1788–1797.
6. Aslan, K.; Lakowicz, J. R.; Geddes, C. D. Rapid Deposition of Triangular Silver Nanoplates on Planar Surfaces: Application to Metal-Enhanced Fluorescence. *J. Phys. Chem. B* **2005**, *109*, 6247–6251.
7. Aslan, K.; Lakowicz, J. R.; Geddes, C. D. Metal-Enhanced Fluorescence Using Anisotropic Silver Nanostructures: Critical Progress to Date. *Anal. Bioanal. Chem.* **2005**, *382*, 926–933.
8. Malicka, J.; Gryczynski, I.; Fang, J.; Kusba, J.; Lakowicz, J. R. Photostability of Cy3 and Cy5-Labeled DNA in the Presence of Metallic Silver Particles. *J. Fluoresc.* **2002**, *12*, 439–447.
9. Peng, H.-I.; Strohsahl, C. M.; Leach, K. E.; Krauss, T. D.; Miller, B. L. Label-Free DNA Detection on Nanostructured Ag Surfaces. *ACS Nano* **2009**, *3*, 2265–2273.
10. Wang, Y.; Liu, B.; Mikhailovsky, A.; Bazan, G. C. Conjugated Polyelectrolyte–Metal Nanoparticle Platforms for Optically Amplified DNA Detection. *Adv. Mater.* **2010**, *22*, 656–659.
11. Cheng, Y.; Stakenborg, T.; Dorpe, P. V.; Lagae, L.; Wang, M.; Chen, H.; Borghs, G. Fluorescence Near Gold Nanoparticles for DNA Sensing. *Anal. Chem.* **2011**, *83*, 1307–1314.
12. Shan, Y.; Xu, J.-J.; Chen, H.-Y. Distance-Dependent Quenching and Enhancing of Electrochemiluminescence from a CdS:Mn Nanocrystal Film by Au Nanoparticles for Highly Sensitive Detection of DNA. *Chem. Commun.* **2009**, *905*–907.
13. Aslan, K.; Zhang, Y.; Hibbs, S.; Baillie, L.; Previte, M. J. R.; Geddes, C. D. Microwave-Accelerated Metal-Enhanced Fluorescence: Application to Detection of Genomic and Exospore Anthrax DNA in <30 seconds. *Analyst* **2007**, *132*, 1130–1138.
14. Sabanayagam, C. R.; Lakowicz, J. R. Increasing the Sensitivity of DNA Microarrays by Metal-Enhanced Fluorescence Using Surface-Bound Silver Nanoparticles. *Nucleic Acids Res.* **2007**, *35*, e13.
15. Fu, Y.; Lakowicz, J. R. Enhanced Fluorescence of Cy5-Labeled DNA Tethered to Silver Island Films: Fluorescence Images and Time-Resolved Studies Using Single-Molecule Spectroscopy. *Anal. Chem.* **2006**, *78*, 6238–6245.
16. Aslan, K.; Huang, J.; Wilson, G. M.; Geddes, C. D. Metal-Enhanced Fluorescence-Based RNA Sensing. *J. Am. Chem. Soc.* **2006**, *128*, 4206–4207.
17. Zhang, J.; Matveeva, E.; Gryczynski, I.; Leonenko, Z.; Lakowicz, J. R. Metal-Enhanced Fluoroimmunoassay on a Silver Film by Vapor Deposition. *J. Phys. Chem. B* **2005**, *109*, 7969–7975.
18. Szmacinski, H.; Murtaza, Z.; Lakowicz, J. R. Time-Resolved Fluorometric Method for One-Step Immunoassays Using Plasmonic Nanostructures. *J. Phys. Chem. C* **2010**, *114*, 7236–7241.
19. Zhang, J.; Fu, Y.; Nowaczyk, K.; Zhao, R. Y.; Lakowicz, J. R. Single-Cell Fluorescence Imaging Using Metal Plasmon-Coupled Probe 2: Single-Molecule Counting on Lifetime Image. *Nano Lett.* **2008**, *8*, 1179–1186.
20. Saha, A.; Basiruddin, S. K.; Sarkar, R.; Pradhan, N.; Jana, N. R. Functionalized Plasmonic-Fluorescent Nanoparticles for Imaging and Detection. *J. Phys. Chem. C* **2009**, *113*, 18492–18498.
21. Zhang, J.; Fu, Y.; Lakowicz, J. R. Fluorescent Metal Nanoshells: Lifetime-Tunable Molecular Probes in Fluorescent Cell Imaging. *J. Phys. Chem. C* **2011**, *115*, 7255–7260.
22. Dulkeith, E.; Ringler, M.; Feldmann, J. Gold Nanoparticles Quench Fluorescence by Phase Induced Radiative Rate Suppression. *Nano Lett.* **2005**, *5*, 585–589.
23. Dulkeith, E.; Morteani, A. C.; Niedereichholz, T.; Klar, T. A.; Feldmann, J. Fluorescence Quenching of Dye Molecules near Gold Nanoparticles: Radiative and Nonradiative Effects. *Phys. Rev. Lett.* **2002**, *89*, 203002.
24. Barazzouk, S.; Kamat, P. V.; Hotchandani, S. Photoinduced Electron Transfer between Chlorophyll *a* and Gold Nanoparticles. *J. Phys. Chem. B* **2005**, *109*, 716–723.
25. Li, Y.-Q.; Guan, L.-Y.; Zhang, H.-L.; Chen, J.; Lin, S.; Ma, Z.-Y.; Zhao, Y.-D. Distance-Dependent Metal-Enhanced Quantum Dots Fluorescence Analysis in Solution by Capillary Electrophoresis and Its Application to DNA Detection. *Anal. Chem.* **2011**, *83*, 4103–4109.
26. Cheng, D.; Xu, Q.-H. Separation Distance Dependent Fluorescence Enhancement of Fluorescein Isothiocyanate by Silver Nanoparticles. *Chem. Commun.* **2007**, *248*–250.
27. Guzatov, D. V.; Vaschenko, S. V.; Stankevich, V. V.; Lunevich, A. Y.; Glukhov, Y. F.; Gaponenko, S. V. Plasmonic Enhancement of Molecular Fluorescence near Silver Nanoparticles: Theory, Modeling, and Experiment. *J. Phys. Chem. C* **2012**, *116*, 10723–10733.
28. Anger, P.; Bharadwaj, P.; Novotny, L. Enhancement and Quenching of Single-Molecule Fluorescence. *Phys. Rev. Lett.* **2006**, *96*, 113002.
29. Chan, Y.-H.; Chen, J.; Wark, S. E.; Skiles, S. L.; Son, D. H.; Batteas, J. D. Using Patterned Arrays of Metal Nanoparticles to Probe Plasmon Enhanced Luminescence of CdSe Quantum Dots. *ACS Nano* **2009**, *3*, 1735–1744.
30. Kulakovitch, O.; Strelak, N.; Yaroshevich, A.; Maskevich, S.; Gaponenko, S.; Nabiev, I.; Woggon, U.; Artemyev, M. Enhanced Luminescence of CdSe Quantum Dots on Gold Colloids. *Nano Lett.* **2002**, *2*, 1449–1452.
31. Bardhan, R.; Grady, N. K.; Halas, N. J. Nanoscale Control of Near-Infrared Fluorescence Enhancement Using Au Nanoshells. *Small* **2008**, *4*, 1716–1722.
32. Zhang, Y.; Aslan, K.; Previte, M. J.; Geddes, C. D. Metal-Enhanced Fluorescence from Copper Substrates. *Appl. Phys. Lett.* **2007**, *90*, 173116.
33. Wang, Y.; Asefa, T. Poly(allylamine)-Stabilized Colloidal Copper Nanoparticles: Synthesis, Morphology, and Their Surface-Enhanced Raman Scattering Properties. *Langmuir* **2010**, *26*, 7469–7474.
34. Pedersen, D. B.; Wang, S. Surface Plasmon Resonance Spectra of 2.8 ± 0.5 nm Diameter Copper Nanoparticles in Both Near and Far Fields. *J. Phys. Chem. C* **2007**, *111*, 17493–17499.
35. Zhu, X.; Wang, B.; Shi, F.; Nie, J. Direct, Rapid, Facile Photochemical Method for Preparing Copper Nanoparticles and Copper Patterns. *Langmuir* **2012**, *28*, 14461–14469.
36. Darugar, Q.; Qian, W.; El-Sayed, M. A.; Pilani, M.-P. Size-Dependent Ultrafast Electronic Energy Relaxation and Enhanced Fluorescence of Copper Nanoparticles. *J. Phys. Chem. B* **2006**, *110*, 143–149.
37. Johnson, P. B.; Christy, R. W. Optical Constants of the Noble Metals. *Phys. Rev. B* **1972**, *6*, 4370–4379.
38. Pastoriza-Santos, I.; Sánchez-Iglesias, A.; Rodríguez-González, B.; Liz-Marzán, L. M. Aerobic Synthesis of Cu Nanoplates with Intense Plasmon Resonances. *Small* **2009**, *5*, 440–443.
39. Wang, H.; Tam, F.; Grady, N. K.; Halas, N. J. Cu Nanoshells: Effects of Interband Transitions on the Nanoparticle Plasmon Resonance. *J. Phys. Chem. B* **2005**, *109*, 18218–18222.
40. Alves, T. V.; Hermoso, W.; Ornellas, F. R.; Camargo, P. H. C. On the Optical Properties of Copper Nanocubes as a

Function of the Edge Length as Modeled by the Discrete Dipole Approximation. *Chem. Phys. Lett.* **2012**, *544*, 64–69.

41. Ye, J.; Verellen, N.; Van Roy, W.; Lagae, L.; Maes, G.; Borghs, G.; Van Dorpe, P. Plasmonic Modes of Metallic Semishells in a Polymer Film. *ACS Nano* **2010**, *4*, 1457–1464.

42. Chowdhury, S.; Bhethanabotla, V. R. Quenching of Fluorescence from CdSe/ZnS Nanocrystal QDs Near Copper Nanoparticles in Aqueous Solution. *Plasmonics* **2011**, *6*, 735–740.

43. Chowdhury, S.; Bhethanabotla, V. R.; Sen, R. Effect of Ag-Cu Alloy Nanoparticle Composition on Luminescence Enhancement/Quenching. *J. Phys. Chem. C* **2009**, *113*, 13016–13022.

44. Oh, M. K.; Baik, H. J.; Kim, S. K.; Park, S. Multiple Surface Plasmon Resonances in Silver and Copper Nanorods. *J. Mater. Chem.* **2011**, *21*, 19069–19073.

45. Kim, D.-K.; Yoo, S. M.; Park, T. J.; Yoshikawa, H.; Tamiya, E.; Park, J. Y.; Lee, S. Y. Plasmonic Properties of the Multispot Copper-Capped Nanoparticle Array Chip and Its Application to Optical Biosensors for Pathogen Detection of Multiplex DNAs. *Anal. Chem.* **2011**, *83*, 6215–6222.

46. Qin, L.-X.; Jing, C.; Li, Y.; Li, D.-W.; Long, Y.-T. Real-Time Monitoring of the Aging of Single Plasmonic Copper Nanoparticles. *Chem. Commun.* **2012**, *48*, 1511–1513.

47. Chan, G. H.; Zhao, J.; Hicks, E. M.; Schatz, G. C.; Van Duyne, R. P. Plasmonic Properties of Copper Nanoparticles Fabricated by Nanosphere Lithography. *Nano Lett.* **2007**, *7*, 1947–1952.

48. Laibinis, P. E.; Whitesides, G. M. Self-Assembled Monolayers of *n*-Alkanethiolates on Copper Are Barrier Films That Protect the Metal against Oxidation by Air. *J. Am. Chem. Soc.* **1992**, *114*, 9022–9028.

49. Jennings, G. K.; Laibinis, P. E. Self-Assembled Monolayers of Alkanethiols on Copper Provide Corrosion Resistance in Aqueous Environments. *Colloids Surf., A* **1996**, *116*, 105–114.

50. Hutt, D. A.; Liu, C. Oxidation Protection of Copper Surfaces Using Self-Assembled Monolayers of Octadecanethiol. *Appl. Surf. Sci.* **2005**, *252*, 400–411.

51. Litorja, M.; Haynes, C. L.; Haes, A. J.; Jensen, T. R.; Van Duyne, R. P. Surface-Enhanced Raman Scattering Detected Temperature Programmed Desorption: Optical Properties, Nanostructure, and Stability of Silver Film over SiO₂ Nanosphere Surfaces. *J. Phys. Chem. B* **2001**, *105*, 6907–6915.

52. Sugawa, K.; Hirono, S.; Akiyama, T.; Yamada, S. Photocurrent Enhancement Tuned with Plasmonic Resonance in Self-Assembled Monolayers Fabricated on Regularly Arranged Gold Nanostructures. *Photochem. Photobiol. Sci.* **2012**, *11*, 318–322.

53. Farcău, C.; Astilean, S. Silver Half-Shell Arrays with Controlled Plasmonic Response for Fluorescence Enhancement Optimization. *Appl. Phys. Lett.* **2009**, *95*, 193110.

54. Mu, W.; Hwang, D.-K.; Chang, R. P. H.; Sukharev, M.; Tice, D. B.; Ketterson, J. B. Surface-Enhanced Raman Scattering from Silver-Coated Opals. *J. Chem. Phys.* **2011**, *134*, 124312-1–124312-7.

55. Stöber, W.; Fink, A.; Bohn, E. Controlled Growth of Monodisperse Silica Spheres in the Micron Size Range. *J. Colloid Interface Sci.* **1968**, *26*, 62–69.

56. Moon, G. D.; Lee, I. T.; Kim, B.; Chae, G.; Kim, J.; Kim, S. H.; M., J.-M.; Jeong, U. Assembled Monolayers of Hydrophilic Particles on Water Surfaces. *ACS Nano* **2011**, *5*, 8600–8612.

57. Kim, T. H.; Kim, H. J.; Lee, T. S.; Lyoo, W. S. Diffraction Color Developed by Self-Assembly of Silica Particle Arrays. *Mol. Cryst. Liq. Cryst.* **2007**, *464*, 153–159.

58. Goss, C. A.; Charych, D. H.; Majda, M. Application of (3-Mercaptopropyl)trimethoxysilane as a Molecular Adhesive in the Fabrication of Vapor-Deposited Gold Electrodes on Glass Substrates. *Anal. Chem.* **1991**, *63*, 85–88.

59. Farcău, C.; Gilioan, M.; Vinteler, E.; Astilean, S. Understanding Plasmon Resonances of Metal-Coated Colloidal Crystal Monolayers. *Appl. Phys. B: Lasers Opt.* **2012**, *106*, 849–856.

60. Kim, J. H.; Ehrman, S. H.; Germer, T. A. Influence of Particle Oxide Coating on Light Scattering by Submicron Metal Particles on Silicon Wafers. *Appl. Phys. Lett.* **2004**, *84*, 1278–1280.

61. Cabrera, N.; Mott, N. F. Theory of the Oxidation of Metals. *Rep. Prog. Phys.* **1948**, *12*, 163–184.

62. Platzman, I.; Brener, R.; Haick, H.; Tannenbaum, R. Oxidation of Polycrystalline Copper Thin Films at Ambient Conditions. *J. Phys. Chem. C* **2008**, *112*, 1101–1108.

63. Hernandez, J.; Wrschka, P.; Oehrlein, G. S. Surface Chemistry Studies of Copper Chemical Mechanical Planarization. *J. Electrochem. Soc.* **2001**, *148*, G389–G397.

64. Akiyama, T.; Miyazaki, A.; Sutoh, M.; Ichinose, I.; Kunitake, T.; Yamada, S. Fabrication of Porphyrin–Titanium Oxide–Fullerene Assemblies on an ITO Electrode and Their Photo-current Responses. *Colloids Surf., A* **2000**, *169*, 137–141.

65. Ichinose, I.; Senzu, H.; Kunitake, T. Stepwise Adsorption of Metal Alkoxides on Hydrolyzed Surfaces: A Surface Sol-Gel Process. *Chem. Lett.* **1996**, *831*–832.

66. Ichinose, I.; Senzu, H.; Kunitake, T. A Surface Sol-Gel Process of TiO₂ and Other Metal Oxide Films with Molecular Precision. *Chem. Mater.* **1997**, *9*, 1296–1298.

67. Araki, K.; Yang, D.-H.; Wang, T.; Selyanchyn, R.; Lee, S.-W.; Kunitake, T. Self-Assembly and Imprinting of Macrocyclic Molecules in Layer-by-Layered TiO₂ Ultrathin Films. *Anal. Chim. Acta* **2013**, *779*, 72–81.

68. Matsuoka, K.; Akiyama, T.; Yamada, S. Step-by-Step Fabrication of Porphyrin–Fullerene Supramolecular Assemblies and Their Photoelectrochemical Properties. *J. Phys. Chem. C* **2008**, *112*, 7015–7020.

69. Chen, Y.; Munehika, K.; Ginger, D. S. Dependence of Fluorescence Intensity on the Spectral Overlap between Fluorophores and Plasmon Resonant Single Silver Nanoparticles. *Nano Lett.* **2007**, *7*, 690–696.

70. Farcău, C.; Astilean, S. Mapping the SERS Efficiency and Hot-Spots Localization on Gold Film over Nanospheres Substrates. *J. Phys. Chem. C* **2010**, *114*, 11717–11722.

71. Techane, S.; Baer, D. R.; Castner, D. G. Simulation and Modeling of Self-Assembled Monolayers of Carboxylic Acid Thiols on Flat and Nanoparticle Gold Surfaces. *Anal. Chem.* **2011**, *83*, 6704–6712.

72. Lahann, J.; Mitragotri, S.; Tran, T.-N.; Kaido, H.; Sundaram, J.; Choi, I. S.; Hoffer, S.; Somorjai, G. A.; Langer, R. A Reversibly Switching Surface. *Science* **2003**, *299*, 371–374.

73. Jennings, T. L.; Singh, M. P.; Strouse, G. F. Fluorescent Lifetime Quenching near $d = 1.5$ nm Gold Nanoparticles: Probing NSET Validity. *J. Am. Chem. Soc.* **2006**, *128*, 5462–5467.

74. Zhang, X.; Marocico, C. A.; Lunz, M.; Gerard, V. A.; Gun'ko, Y. K.; Lesnyak, V.; Gaponik, N.; Susha, A. S.; Rogach, A. L.; Bradley, A. L. Wavelength, Concentration, and Distance Dependence of Nonradiative Energy Transfer to a Plane of Gold Nanoparticles. *ACS Nano* **2012**, *6*, 9283–9290.

75. Luo, S.; Zhang, E.; Su, Y.; Cheng, T.; Shi, C. A Review of NIR Dyes in Cancer Targeting and Imaging. *Biomaterials* **2011**, *32*, 7127–7138.

76. Benson, R. C.; Kues, H. A. Fluorescence Properties of Indocyanine Green as Related to Angiography. *Phys. Med. Biol.* **1978**, *23*, 159–163.

77. Tam, F.; Goodrich, G. P.; Johnson, B. R.; Halas, N. J. Plasmonic Enhancement of Molecular Fluorescence. *Nano Lett.* **2007**, *7*, 496–501.

78. Aslan, K.; Lakowicz, J. R.; Geddes, C. D. Rapid Deposition of Triangular Silver Nanoplates on Planar Surfaces: Application to Metal-Enhanced Fluorescence. *J. Phys. Chem. B* **2005**, *109*, 6247–6251.

79. Sugawa, K.; Kawahara, T.; Akiyama, T.; Kobayashi, M.; Takahara, A.; Yamada, S. Enhanced Absorption and Emission in a Copper Phthalocyanine–Gold Nanoparticle System Assisted by Localized Surface Plasmon. *Chem. Lett.* **2009**, *38*, 326–327.

80. Canesi, E. V.; Capsoni, M.; Karnam, L.; Lucotti, A.; Bertarelli, C.; Zoppo, M. D. Solution Processed, Versatile Multilayered Structures for the Generation of Metal-Enhanced Fluorescence. *J. Phys. Chem. C* **2013**, *117*, 13197–13201.

81. Pompa, P. P.; Martiradonna, L.; Torre, A. D.; Sala, F. D.; Manna, L.; Vittorio, M. D.; Calabi, F.; Cingolani, R.; Rinaldi, R. Metal-Enhanced Fluorescence of Colloidal Nanocrystals with Nanoscale Control. *Nat. Nanotech.* **2006**, *1*, 126–130.

82. Nooney, R. I.; Stranik, O.; McDonagh, C.; MacCraith, B. D.; Gabudean, A. M.; Focsan, M.; Astilean, S. Gold Nanorods Performing as Dual-Modal Nanoprobes *via* Metal-Enhanced Fluorescence (MEF) and Surface-Enhanced Raman Scattering (SERS). *J. Phys. Chem. C* **2012**, *116*, 12240–12249.
83. Lohmüller, T.; Iversen, L.; Schmidt, M.; Rhodes, C.; Tu, H.-L.; Lin, W.-C.; Groves, J. T. Single Molecule Tracking on Supported Membranes with Arrays of Optical Nanoantennas. *Nano Lett.* **2012**, *12*, 1717–1721.
84. Ozel, T.; Mizamoglu, S.; Sefunc, M. A.; Samarskaya, O.; Ozel, I. O.; Mutlugun, E.; Lesnyak, V.; Gaponik, N.; Eychmuller, A.; Gaponenko, S. V.; Demir, H. V. Anisotropic Emission from Multilayered Plasmon Resonator Nanocomposites of Isotropic Semiconductor Quantum Dots. *ACS Nano* **2011**, *5*, 1328–1334.
85. Lakowicz, J. R.; Shen, B.; Gryczynski, Z.; D'Auria, S.; Gryczynski, I. Intrinsic Fluorescence from DNA Can Be Enhanced by Metallic Particles. *Biochem. Biophys. Res. Commun.* **2001**, *286*, 875–879.
86. Zhang, Y.; Dragan, A.; Geddes, C. D. Wavelength Dependence of Metal-Enhanced Fluorescence. *J. Phys. Chem. C* **2009**, *113*, 12095–12100.
87. Fu, Y.; Zhang, J.; Lakowicz, J. R. Largely Enhanced Single-Molecule Fluorescence in Plasmonic Nanogaps Formed by Hybrid Silver Nanostructures. *Langmuir* **2013**, *29*, 2731–2738.
88. Yuan, C. T.; Wang, Y. C.; Cheng, H. W.; Wang, H. S.; Kuo, M. Y.; Shih, M. H.; Tang, J. Modification of Fluorescence Properties in Single Colloidal Quantum Dots by Coupling to Plasmonic Gap Modes. *J. Phys. Chem. C* **2013**, *117*, 12762–12768.
89. Fu, Y.; Zhang, J.; Lakowicz, J. R. Large Enhancement of Single Molecule Fluorescence by Coupling to Hollow Silver Nanoshells. *Chem. Commun.* **2012**, *48*, 9726–9728.
90. Kim, K.-S.; Kim, H.; Kim, J.-H.; Kim, J.-H.; Lee, C.-L.; Laquai, F.; Yoo, S. I.; Sohn, B.-H. Correlation of Micellar Structures with Surface-Plasmon-Coupled Fluorescence in a Strategy for Fluorescence Enhancement. *J. Mater. Chem.* **2012**, *22*, 24727–24733.
91. Zhang, J. H.; Zhan, P.; Wang, Z. L.; Zhang, W. Y.; Ming, N. B. Preparation of Monodisperse Silica Particles with Controllable Size and Shape. *J. Mater. Res.* **2003**, *18*, 649–653.